The $Na_2FeP_2O_7$-carbon nanotubes composite as high rate cathode material for sodium ion batteries

Gianluca Longoni[a]

Ji Eun Wang[b]

Young Hwa Jung[b]

Do Kyung Kim[b]

Claudio M. Mari[a]

Riccardo Ruffo[a, *]

riccardo.ruffo@unimib.it

[a]Department of Materials Science, Università degli Studi di Milano-Bicocca, Via Cozzi ~~53~~55, 20125 Milano, Italy

[b]Department of Materials Science and Engineering, Korea Advanced Institute of Science and Technology (KAIST), 291 Daehak-ro, Yuseong-gu, Daejeon 305-701, Republic of Korea

*Corresponding author.

Abstract

Among the viable positive electrode materials recently proposed for Na-ion secondary batteries, $Na_2FeP_2O_7$ was investigated thanks to its facile preparation, the use of highly abundant and low cost raw materials, and the highest thermal stability among all others cathode materials. In the present work the electrochemical features of the $Na_2FeP_2O_7$ are improved by synthesizing a $Na_2FeP_2O_7$-carbon nanotubes composite with prominent high-rate performances. The material shows a reversible specific capacity of 86 mAh g^{-1} for 140 cycles at 1C and 68 mAh g^{-1} at 10C. An in depth investigation about the Na^+ diffusion rates inside the material was conducted by electrochemical impedance spectroscopy.

Keywords: Iron pyrophosphate; Composite electrodes; Multi walled carbon nanotubes; Sodium ion batteries

1 Introduction

During the last 20 years, Li-ion rechargeable batteries (LIBs) have become a mature and reliable technology. Their main qualities reside in the high energy density (120–150 W h dm^{-3} [1]), the lightweight, the remarkable round-trip efficiency, and high power [2,3]. These predominant characteristics have made LIBs the best choice for a wide range of applications: from electric cars (Electric vehicle and hybrid electric vehicle) to high-end portable electronics (smart phones, laptops and entertainment electronics). Nevertheless, some aspects are considered matter of concern for a further spread of LIB technology. In a worst-case scenario pictured by some scientists [4], the accessible amount of raw materials is a major limitation to the complete penetration of LIBs in the automotive market, for example. In more optimistic landscapes, the energetic cost~~s~~ related to LIBs materials manufacturing is a primary concern [5]. Sustainability of material processing gains more and more relevance in grid application, where a cut in the costs is advantageous for the marketability of reliable high capacity systems. For these reasons Na-ion batteries have attracted an increasing attention due to the higher availability of raw materials and the possibility to drive down the energetic demand connected to raw materials extraction and processing. The most relevant technological obstacle that has to be overcome in sodium-ion technology is the chemical-physical limit coming from the higher hindrance of the sodium cation [6]. For this reason a new series of tailored anode and cathode materials has been proposed [6,7]. Several cathode materials have been investigated so far by many groups. Amongst the most promising, worthy to be mentioned are the layered-structured TMs (transition metals) oxides such as Na_xCoO_2 [8], Na_xVO_2 [9], $Na_x(Fe_{1/2}Mn_{1/2})O_2$ [10] and $Na(Mn_{1/3}Co_{1/3}Ni_{1/3})O_2$ [11] capable of storing between 100 and 200 mAh g^{-1}. A series of polyanionic compounds has been widely investigated as well. Some of the most recent works about these compounds describe the promising performances of $Na_3V_2(PO_4)_3$ [12] and $Na_4M_3(PO_4)_2(P_2O_7)$ with M = Fe, Co [13,14]. They show an operational potential ranging from 2.5 to 4.5 V vs. Na/Na^+, and capacities between 80 and 100 mAh g^{-1}. In order to keep the manufacturing cost as low as possible, the attention has been addressed to low cost Na–Fe–P–O systems. In particular pyrophosphates have been taken into account considering their thermal stability and the relative facile process of preparation. Pyrophosphate compounds ($M_xP_2O_7$) originate from the heat treatment of phosphates under reducing condition (H_2/Ar mixture), so that oxygen is thermodynamically prompted to abandon the phosphate lattice, creating oxygen-poor units: P_2O_7 or $(PO_{4-x})_2$ [15]. Furthermore, the lithium analog compound, $Li_2FeP_2O_7$,

demonstrated itself to be thermally stable up to 1400 °C, much more than phosphates that undergo decomposition at 700 °C [15]. High performance pyrophosphates ($Na_2FeP_2O_7$) preparation routes already investigated, include highly energetic ceramic methods [16,17] and solid state synthesis [18]. These methods, beside to the advantage of the crystalline phase fine control, have the drawback of the highly energetic steps involved in precursors processing, such has high temperature heat treatments and ball-milling. A low cost, soft-chemistry synthetic approach to a high performance $Na_2FeP_2O_7$ cathode, still is missing. For what concern electronic conductivity of pyrophosphate, other than iron pyrophosphate, many studies have been carried out, and specifically for transition metal pyrophosphate, a mild mixed ionic-electronic conductivity has been proposed [19]. This not-so-high electronic conductivity has been attributed also to $Na_2FeP_2O_7$ and has been tackled using different approaches such as down-sizing the particles dimension, carbon-coating the $Na_2FeP_2O_7$ particles [20], or, ultimately, increasing the carbonaceous (carbon black) conductive matrix in the electrode formulation.

In light of these considerations, a $Na_2FeP_2O_7$/multiple-walled carbon nano tubes (MWCNT) composite has been prepared using an aqueous synthesis followed by a mild thermal treatment, and has been evaluated as a promising material for low-cost and kinetically-performing cathode material for Na-ion batteries. In order to overcome the intrinsic low conductive nature of the material, a new perspective has been employed for this material: a multiple walled carbon nanotubes network has been used as growing substrate for the material. Low percentages of multiple walled nanotubes have been chosen instead of pricier materials (single walled nanotubes or graphene) to keep the overall preparation process economically affordable. A facile and easy-to-reproduce synthetic path has been employed, and an exhaustive electrochemical characterization of the composite has been carried out in order to provide evidences of the benignity of $Na_2FeP_2O_7$/MWCNT as a viable and trustworthy cathode material for sodium ion batteries based on an organic electrolyte solution. Added to this, electrochemical impedance spectroscopy has been used in calculating, for the first time, the sodium diffusion coefficient inside $Na_2FeP_2O_7$ phase, providing further proofs of the benignity of the material and giving experimental justification to theoretic considerations made elsewhere [21].

2 Experimental section

2.1 Materials synthesis

In order to present an organic and thorough work, two different batches have been prepared: a pure $Na_2FeP_2O_7$ compound batch has been addressed as a reference material, while a $Na_2FeP_2O_7$/MWCNT composite with a nominal 10% concentration in weight of MWCNTs (6–9 nm × 5 µm, >95%, Sigma Aldrich®) was considered the main term of comparison. The synthetic route, in both cases, was kept the same. For the preparation of pristine $Na_2FeP_2O_7$, $Fe(NO_3)_3{\cdot}9H_2O$ (ACS reagent, ≥98%, Sigma Aldrich®) was firstly dissolved in 100 mL deionized water under vigorous magnetic stirring (400 RPM). $H_2C_2O_4{\cdot}2H_2O$ (ACS reagent, ≥99%, Sigma Aldrich®) was added, obtaining a weary turn of the solution color from a robust orange to a faint yellow. Subsequently, $NH_4H_2PO_4$ (ACS reagent, ≥99.0%, Fluka) was added, and after that, Na_2CO_3 (ACS reagent, ≥99.5%, Alfa Aesar®) was dissolved as the sodium precursor. The temperature of the stirred solution was then set to 80 °C, and the solvent was evaporated completely (6–10 h) until a dense yellow paste was obtained by coprecipitation of mixed Na and Fe cations phosphate. All the precursors were used as obtained without further purification. The product was recovered and dried at 100 °C inside an oven overnight. For the synthesis of the other composite, the process was the same apart from the slow dropping of a water-based suspension of carbon nanotubes (MWCNT) just before the raise in the temperature of the solution. The amount of carbon nanotubes added in the composites synthesis was calculated in order to achieve the desired final nominal concentration of 10% by weight. For clarity, the composite will be referred as NFPy/MWCNT, while the sample with no nanotubes, as NFPy. A heat treatment was disposed for all the batches by putting the powders into an alumina crucible and housing it inside a quartz sealed tube. The tube, equipped with gas inlet/outlet, was connected to 5% H_2/Ar (Sapio®) gas mixture line and was then placed into a tubular oven (Carbolite). The temperature program was constituted by a ramp through which the sample was heated at 5 °C min^{-1} to 600 °C, and kept at that temperature for 10 h. During the whole heat treatment a steady 70 cc min^{-1} flow of the H_2/Ar mixture was provided. The as obtained materials were subjected to different chemical-physical characterizations.

2.2 Structural and physical characterization

Morphological characterizations of as-prepared materials were analyzed by both SEM (HITACHI, S-4800) and TEM (FEI, Tecnai G^2 F30 S-Twin). Elemental analysis was performed using a FLASH 2000 series (Thermo Scientific) in order to assess the amount of carbon included in the $Na_2FeP_2O_7$/MWCNT composite and to evaluate the entity of other impurities. High resolution X-ray powder diffraction pattern was collected from a Rigaku diffractometer (D/Max-2500). Diffraction patterns were acquired in the 2θ window between 5° and 70°, at 4° min^{-1} scan rate.

2.3 Electrochemical characterization

The Galvanostatic Cycling under Potential Limitation technique (GCPL) was employed to evaluate the electrochemical behavior of the materials. Electrodes were prepared by casting a dense slurry composed by the active material (NFPy or NFPy/MWCNT), a carbonaceous matrix (Carbon Black) and the binder (PVDF, Solvay® 6020) suspended in the minimum amount of 1-methyl-2-pyrrolidinone, onto an aluminum foil (30 µm thick). The proportion among the components of the slurry was 75:17:8 by weight, respectively. After the casting, the wet film was let to cure in an oven at 80 °C under vacuum. 9 mm and 16 mm diameter disks were punched out from the dried film, and three-electrodes Swagelok-type cells and two-electrodes CR2032 coin cell type cells were assembled in an Ar-filled glove box (Mbraun) using a sodium disk as reference and counter electrodes. The two different cell configurations were employed in order to perform different tests, depending on the more suitable set up (two or three electrodes) for the experiment itself: for instance, GCPLs were performed assembling two-electrodes coin cells while EIS measurements required a three electrodes set up. The material load deposited on each electrode was calculated to be around 1 mg cm^{-2} and the final thickness of the deposition was determined as 20 µm. On every electrode the precise amount of the active material ($Na_2FeP_2O_7$) has been esteemed by mean of a 1/100 mg resolution laboratory scale (MettlerToledo). During each cell assembly, a glass fiber disk soaked in the electrolyte solution was employed as the separator between positive and negative electrode. The electrolyte solution employed was obtained by dissolving $NaClO_4$ (ACS reagent, ≥98%, Sigma–Aldrich®) in propylene carbonate (≥99.9%, Merck) to

obtain a 1 M solution, and adding 2% by weight of fluoroethylene carbonate (99%, Aldrich®). Together with single C rate Galvanostatic Cycling under Potential Limitation (GCPL) tests, experiment at progressively increasing C rates was also performed. Galvanostatic intermitted titration technique (GITT) and Potentio-Electrochemical impedence spectroscopy (PEIS) tests were performed on the three electrodes configuration Swagelok cell, at different temperatures, using a thermostatic chamber (ACS test chamber). For the impedance measurements, a bias voltage of 10 mV was applied and each was scanned between 200 kHz and 0.05 Hz. For all the electrochemical tests a VSP-300 BioLogic galvanostat/potentiostat was employed.

3 Results and discussion

3.1 Chemical-physical characterization

SEM micrographs of the as synthesized materials are reported in Fig. 1. It can be seen how micrometric sized particles were obtained from the synthetic route described above. The main difference between the two samples resides in the average dimension of the particles, which was considerably lower in the case of NFPy/MWCNT. For what concerns NFPy, large globular agglomerates larger than 5 μm with a relative rough surface can be observed. On the other hand, Carbon nanotubes partially embedded in smaller and rougher NFPy/MWCNT particles can be easily spotted in Fig. 1d. From both SEM and TEM pictures, the distribution of nanotubes can be assessed as homogeneous inside the sample. Despite the crystalline nature of the samples highlighted by the XRD diffraction patterns showed below, electrons diffraction lattice fringes can be hardly seen in high magnification TEM images c and f in the same Fig. 1, due to the high 3D domain of the particles. Starting from what can be seen in NFPy/MWCNT SEM micrographs, a nucleation and a growth of sodium iron pyrophosphate precursor particles around nanotubes flakes can be hypothesized. In order to precisely evaluate the accurate amount of nanotubes inside NFPy/MWCNT sample, an elemental analysis was performed and the results reported in Table 1. The real amount of carbon sensed inside NFPy/MWCNT sample was evaluated to be 7.15% by weight. In first approximation it has been all addressed to nanotubes content, and it will be taken into consideration in the future calculation involving the real amount of the electrochemical active material, namely the sodium iron pyrophosphate alone. In this concentration, MWCNT can be considered not to heavily influence the overall production costs of the material, owing also the relative lower value of multiple carbon nanotubes compared to single walled carbon nanotubes or graphene, utilized as conductive matrixes as well. Carbon content in NFPy is below 0.2% and can be addressed to carbon residues coming from precursors employed during the synthesis, such as oxalic acid and sodium carbonate. The distribution of constitutive elements of the compounds has been evidenced by EDS elemental mapping reported in Fig. 2. No preferential segregation of elements is observed, symptom of the coprecipitation synthetic process benignity.

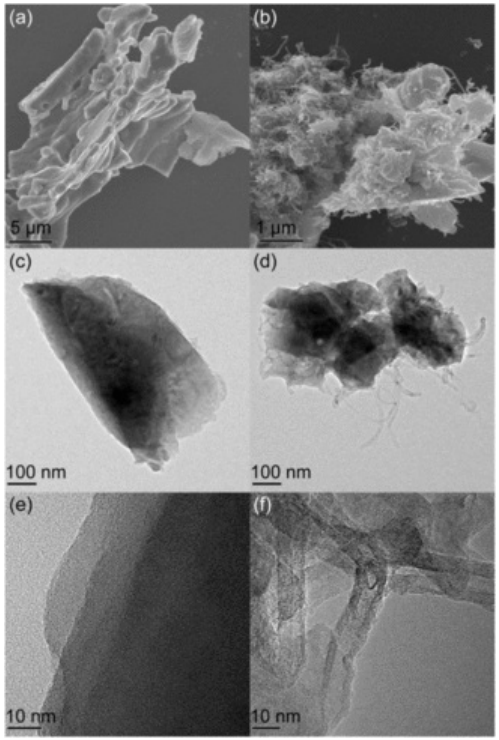

Fig. 1 SEM micrographs of as synthesized a) NFPy and b) NFPy/MWCNT. TEM images at increasing magnification of b), c) NFPy and e), f) NFPy/MWCNT composite.

Table 1 Elemental analysis of NFPy and NFPy/MWCNT.

	NFPy	NFPy/MWCNT
Nitrogen	0.09185 ± 0.0001	0.05199 ± 0.0002
Carbon	0.16496 ± 0.0017	7.14635 ± 0.0374
Hydrogen	0.07936 ± 0.0001	0.09824 ± 0.0001
Sulfur	0.06681 ± 0.0013	0.04024 ± 0.0001

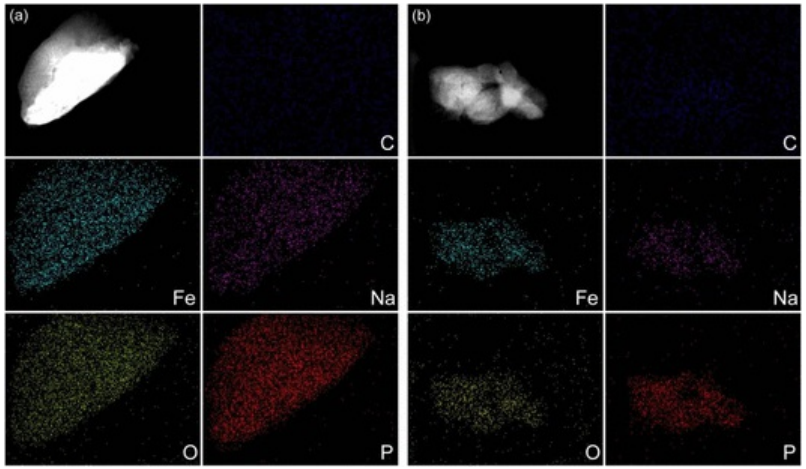

Fig. 2 STEM images and EDS elemental mapping of (a) as-synthesized NFPy and (b) NFPy/MWCNT particles.

From the diffraction patterns reported in Fig. 3, the highly crystalline nature of the two samples can be noticed. In the same picture, the reference peaks calculated from the Rietveld refinement reported elsewhere [22] are shown, so that the correspondence between the diffraction signals of the obtained compounds and reference data can be appreciated. On this basis the crystal structure was evaluated to have a triclinic unit cell, in a configuration ascribable to the *P-1* space group (No. 2). In this arrangement, a continuous frame made of FeO_6–FeO_6 and PO_4–PO_4 corner and edge-sharing units [15] creates an infinite 3-D network, in whose channels the Na cations can easily diffuse. This crystalline structure is iso-structural with other pyrophosphate already investigated in literature, such as $Na_2CoP_2O_7$ [23].

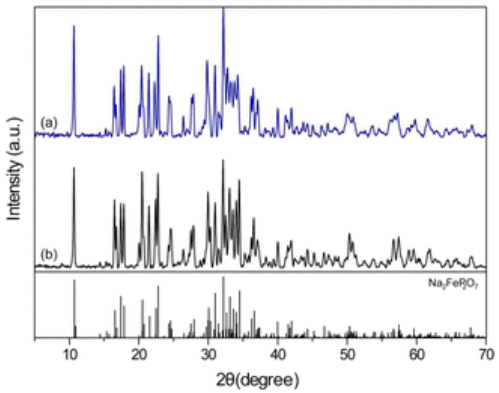

Fig. 3 Diffraction pattern of NFPy (black line) and NFPy/MWCNT composite (blue line). (For interpretation of the references to colour in this figure legend, the reader is referred to the web version of this article.)

3.2 General electrochemical characterization

A conspicuous number of different electrochemical tests were performed in order to draw attention to limits and qualities of the prepared materials. In Fig. 4a, the intrinsic limit of NFPy alone is highlighted. While NFPy/MWCNT is being charged and discharged for more than 60 cycles, without recording almost any substantial loss in capacity, the capacity extracted from NFPy electrode is considerably lower and it fades consistently during the first 20 cycles, reaching 23 mAh g^{-1} at the 50th cycle. On the contrary, NFPy/MWCNT composite ensures a capacity close to 85 mAh g^{-1}, for more than 60 cycles, equal to 87.6% of the theoretical specific capacity for the material (97 mAh g^{-1}). This value is comparable with data reported in literature registered at the same current (1 C) in the same experimental condition [24], nevertheless a Coulombic efficiency of 99.8% ± 0.25, averaged over 60 cycles, has never been reported in literature for this material. It might be interesting to compare also the performance of the NFPy/MWCNT composite material when formulated as electrode with or without the carbon black additive (Fig. 4b). In this latter case the electrode deliver a stable capacity of 68 mA h/g at C1. A full optimization of electrode properties is far behind the aim of this paper, however it is clear that the MWCNTs presence is essential to stabilize the properties over cycling while only the interaction between MWCNTs and carbon black particles creates an efficient electrical network able to exploit the active material full capacity at high rate (see also the discussion of Fig. 6). Charge/discharge profiles of the NFPy/MWCNT are shown in Fig. 4c. At the end of the very first charging process (black upward curve), a capacity above 86 mAh g^{-1} is reached (1C), which means that the starting condition of $Na_{2-x}Fe^{II}_{1-x}Fe^{III}_{x}P_2O_7$, is addressable to an almost completely sodiated (x = 0) material. The voltage profile of the same curve shows a first plateau around 2.5 V and a longer second one at 3.0 V. Two slight humps are also noticeable around 3.1 and 3.2 V, and their possible nature will be discussed later on in this work. A substantial difference between discharge voltage profile (downward curves) of first cycles (up to the 10th) and the following decades can be noticed. It is related to the additional step at 2.9 V that progressively disappear through cycles. Since it doesn't have its counterpart in the charge profile, this was addressed to an irreversible structural change towards the most stable iron pyrophosphate phase. The 5th cycles of cyclic voltammograms obtained at different scan rates are reported in Fig. 5. At around 2.5 and 3.0 V, it can be recognized the peaks correlated to the two main plateaus obtained in the galvanostatic cycling. Worthy to be noted is the extremely low polarization, even at high scan rate, compared to CVs reported in literature for the same material [22]. To be more precise, the peaks centered at around 3.2 V create a set of three different signals (at 2.92, 3.04 and 3.18 V) accounting for a series of different mechanisms occurring during the main intercalation process, embodied by the plateau at 3.0 V in the GCPL. A small peak at 3.21 V can be noted as well, especially at low scan rate (inset of Fig. 5). According to DFT calculation reported elsewhere [20], the peak at 2.52 V (anodic curve at a scan rate of 0.5 mV s^{-1}) refers to the more thermodynamically and kinetically accessible Na to be extracted from pyrophosphate lattice. Signals at higher potentials, instead, all refer to Na extraction mechanisms occurring at comparable activation energies, and differentiating from one another depending on the slight differences in de-intercalation/intercalation pathways. 1D and/or 2D paths are involved in this phase, as reported in simulated structures [21].

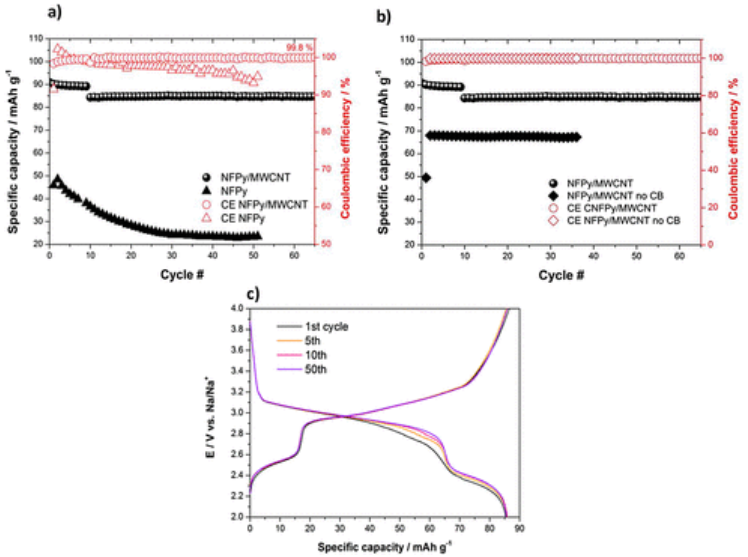

Fig. 4 Capacity retention tests for a) NFPy and NFPy/MWCNT at 1 C(the first 10 cycles for NFPy/MWCNT composite have been recorded at C/10 the rest at 1 C) and b) NFPy/MWCNT electrodes fabricated with and without carbon black; c) charge and discharge profiles of NFPy/MWCNT composite recorded cycling the electrode at 2 C (97 mA g^{-1}).

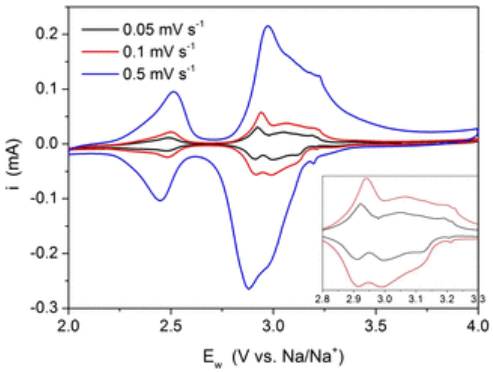

Fig. 5 Cyclic voltammograms of NFPy/MWCNT electrode obtained at different scan rates.

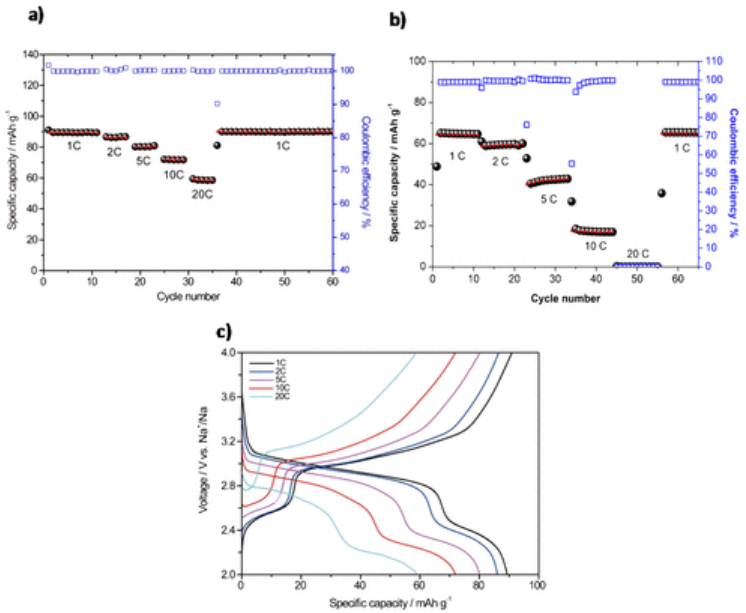

Fig. 6 Rate capability tests: a) NFPy/MWCNT electrode fabricated with carbon black; b) NFPy/MWCNT electrode fabricated without carbon black; c) charge discharge profiles of NFPy/MWCNT electrode fabricated with carbon black.

A rate test of the most promising material, namely NFPy/MWCNT, is reported in Fig. 6. Even at high current rates (10 C), more than 60 mAh g^{-1} of discharge capacity was achieved. Capacity value extracted at 10 C (70 mAh g^{-1}) is comparable with the one reported in the work by Chen et al. [25], in which a more stable and reliable ionic liquid based electrolyte has been employed. This aspect is highly welcomed considering that, even not using an optimized and costly electrolyte solution, the material, object of this work, shows high stability and valuable kinetic properties, with more than 50 mAh g^{-1} capacity at 20 C. Added to this, using a PC $NaClO_4$ solution, no temperature increase is needed to bring the IL to a suitable level of viscosity in order not to slow down the diffusion processes inside the cell [24]. This is a value considerably higher than those reported in literature referring to test conducted in the same conditions [26]. Added to this promising performance, the cells assembled and tested at increasing C-rates do not show appreciable losses in capacity if brought back to low rates (1 C). An efficient and fast process kinetics coupled to a general stability of the material and of the SEI layer can be assumed, as also proved by the charge/discharge profiles (Fig. 6c). On the other part, the electrode fabricated without the carbon black additive shows stable capacity, as already pointed out but slower kinetic properties at current higher than 2C (Fig. 6b). The electrical network created by the interconnection between CB particles and MWCNT is essential to exploit the material properties at high rate.

3.3 EIS measurements

To deepen the understanding of the electrochemical behavior of the two materials investigated, a plenty of EIS tests have been conducted. The cell set up employed during the analysis was a three electrode Swagelok-like cell assembly. For the whole duration of the EIS tests, the cells were kept in a climatic chamber with the possibility of a fine temperature and humidity conditions control (±0.1 °C and ±0.1% of relative humidity). The same thermostatic chamber was also useful to perform EIS analysis at different temperatures, which was conducted in order to assess the entity of thermally activated processes. All the tests were conducted after a 5-charge/discharge cycles of each cell, ending up at an SOC of 0.5 (~3.0 V vs. Na/Na^+). In Fig. 7a, EIS spectra for both NFPy/MWCNT and NFPy electrodes obtained at 25 °C are reported. Solid and dashed black lines superimposed to experimental data refer to the equivalent circuit fitting. Due to the substantial difference between the two signals, two different equivalent circuits have been taken into consideration. In the case of NFPy/MWCNT, where different RCs contribution can be easily deconvoluted, circuit 1 (inset of Fig. 7) was considered. It was built up starting from a common Randles-like circuit, and adding a further $R_{int}C_{int}$ parallel in series between the resistance accounting for the solution IR drop (R_s) and the $R_{ct}C_{dl}$ with the Warburg element (W). In this way the separation between the particles interfacial resistance, capacitance (correlated to Na^+ desolvation and extended double layer capacitance), charge transfer process and double layer capacitance was obtained. This kind of equivalent circuit was already taken into account to model several types of battery chemistries [27,28]. In the NFPy case, a simple Randles circuit was employed (circuit 2 in the inset of Fig. 7) due to the complexity of deconvolution of processes having similar time domains. In each circuit, every capacitor has been substituted by a Constant Phase Element (CPE) to overcome the deviation from a capacitance ideal behavior. A pure Warburg element has been considered in both circuits in order to model the solid phase semi-infinite Na^+ diffusion in the intercalating material. It should be noted that extending the analysis frequencies to very low frequency values (0.5 mHz), a deviation from a pure Warburg signal is commonly obtained (Fig. 7b) [29]. In this case, a Modified Restricted Diffusion element would have been more suitable to model the Na^+ diffusion inside the active material in series with a physical blockage to a further diffusion due to the presence of the aluminum current collector, in which Na alloying is not possible. Nevertheless, we felt legitimate to exclude this low frequencies region, since the main interest was to discuss Na diffusive properties in the active material by Warburg Z_D impedance values analysis.

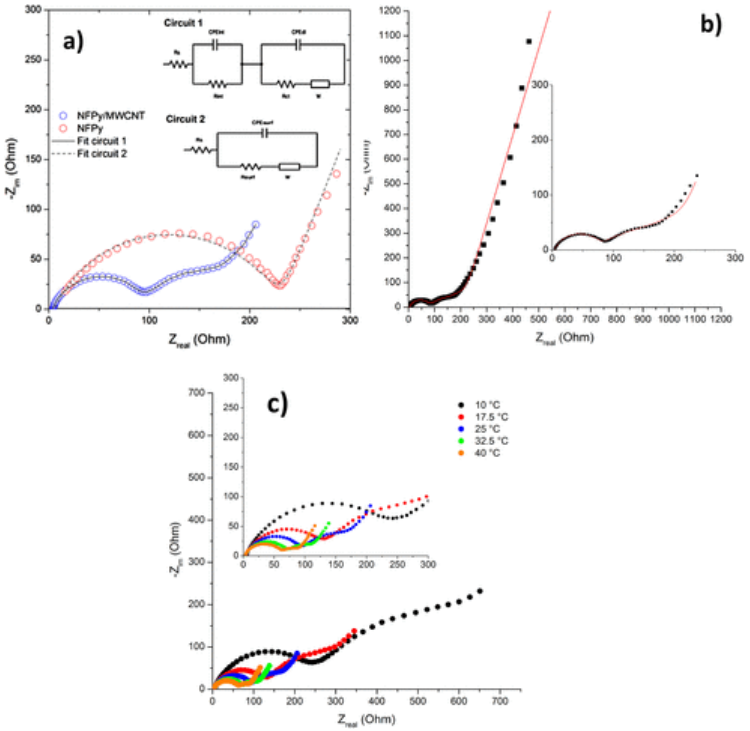

Fig. 7 EIS tests set composed by (a) Nyquist plot of NFPy/MWCNT and NFPy electrodes. In black lines are reported the equivalent circuits fitting curves and in the inset are reported schematically the related equivalent circuits. (b) Nyquist plot of NFPy/MWCNT EIS analysis, having the frequencies window extended to 0.5 mHz, in order to highlight the deviation from the pure warburg ~~behaviour~~ behavior at mid-low frequencies. (c) EIS spectra conducted at different temperature (SOC 0.5). Inset refers to mid-high frequency range.

Experimental data obtained from the fitting are reported in Table 2. In order to make a first comparison between the materials possible, NFPy/MWCNT R_{int} and R_{ct} values were summed and compared to the surface resistance value (R_{surf}) obtained from NFPy electrode impedance analysis. From these values, the beneficial effect of the addition of carbon nanotubes can be noted. The lower resistance (177 Ω) for NFPy/MWCNT sample can be attributed to a more efficient electric connection of particle–particle and particle-conductive matrix rather than to a more effective charge transfer process, considering the similar nature of the active materials. The sodium diffusion coefficient (D_{Na}) in the solid solution, was calculated from the Warburg impedance values (Z_D) reported in Table 2 according to the following equations [28,30,31]:

$$Z_D = V_m \frac{\left(dE/dx\right)}{n F D_{Na}^{\frac{1}{2}} A}$$

Table 2 Results of electrochemical impedance spectroscopy analysis.

	NFPy/MWCNT	NFPy
R_s/Ω	5~~.495~~	5~~4.52~~
R_{int}/Ω	92	–
R_{ct}/Ω	85	–
R_{surf}/Ω	177	224
Z_D	32~~31.77~~	111~~110.6~~

From which, rearranging, we obtain

$$D_{Na} = \left[\left(\frac{V_m}{n F Z_D A}\right)\left(\frac{dE}{dx}\right)\right]^2$$

~~Where~~ where V_m is the molar volume of the species $Na_2FeP_2O_7$, calculated from the SXRD Rietveld refinement data reported in literature for the same crystalline phase [15], n is the number of electrons exchanged for Na atom, F is the Faraday constant, A is the electrode material active area, and (dE/dx) is the slope of the equilibrium potential versus composition. This latter value was obtained from a Galvanostatic Intermittent Titration technique (GITT) conducted on the same electrode using 5 mAh g^{-1} impulses at 0.5 C, and a resting period of 30 min after each impulse. The value of D_{Na} obtained at 25 °C was 8.45×10^{-13} cm^2 s^{-1}. It is one order of magnitude higher than diffusion coefficient values of Na in oxides, such as $Na_{0.44}MnO_2$ [28] and two order of magnitude higher than Li ion diffusion inside iron pyrophosphate measured at the same SOC, as reported in a recent work by Deng et al. [32] in which $Li_2FeP_2O_7$ was synthesized in a monoclinic structure (space group: $P2_1/C$) providing a 2D diffusion network for Li^+ diffusion. Doing the same calculation for pristine NFPy, a Na diffusion coefficient of 2.79×10^{-13} cm^2 s^{-1} was obtained. This discrepancy with the previous value might be attributed to morphological differences of the particles induced by nanotubes-driven growing process. These somewhat high diffusion coefficients, reported for sodium iron pyrophosphate here for the first time as far as we know, are consistent with the structural and diffusive properties of sodium iron pyrophosphate theoretically discussed elsewhere. In the work by Barpanda et al. [21], it is pointed out how the FeO_6 octahedra and PO_4 tetrahedra are interconnected in a staggered fashion, creating large 3D pathways in which alkali ions (Na^+) can easily diffuse despite their dimension, with modest activation energies (0.49 eV for Na^+ in $Na_2FeP_2O_7$). These values are generally higher than the corresponding values in other intercalating materials such as $LiFePO_4$ and $NaFePO_4$ in which alkali atoms diffusion follow a stricter 1D path [33].

In Fig. 7c, NFPy/MWCNT EIS spectra collected at different temperature are reported. For each temperature step, after increasing the temperature (using a liner program with a slope of 0.5 °C min^{-1}), the system was allowed equilibrating for 1 h before registering the impedance. OCV was monitored during this resting period. The temperature window investigated ranged from 10 °C to 40 °C with 7.5 °C steps. As can be appreciated from the Nyquist plot, EIS signals show substantial differences. Table 3 displays the values for R_s, R_{int} and R_{ct} extrapolated at different temperatures. As can be easily noted, all the resistance values decrease as the temperature rises in a fashion that leads R_{int} and R_{ct} to be comparable at 25 °C. In Fig. 8b, it can be spotted the Arrhenius dependence between resistance values and temperature, suggesting the thermally activated nature of interfacial sodium diffusion and charge transfer mechanism. The values of i_0, exchange current for the charge transfer process, were calculated from R_{ct}, considering the approximation of the Butler–Volmer relation for small overpotentials:

$$i_0 = \frac{R T}{R_{ct} n F}$$

Table 3 Temperature dependence of electrode resistances.

	Temperatures/K				
	283.15	290.65	298.15	305.65	313.15
R_s/Ω	6~~.35~~	5~~.26~~	4~~.52~~	4~~3.95~~	4~~3.65~~
R_{int}/Ω	250~~249.7~~	127	92	68~~67.55~~	58~~.5~~
R_{ct}/Ω	427~~426.8~~	194~~193.7~~	85~~.02~~	46~~45.74~~	29~~.45~~

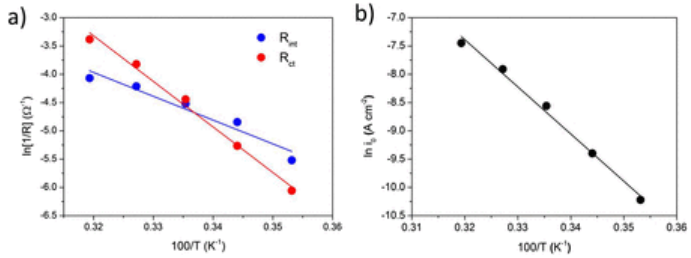

Fig. 8 Arrhenius plot for a) resistance values related to interface resistance and charge transfer resistance, and b) exchange current i_0.

From the $\ln(i_0)$ vs. 100/T plot slope, the activation energy E_a for the charge transfer process has been calculated. i_0 values range from 36 to 583 μA cm^{-2} at 10 °C and 40 °C respectively and the related value of E_a was 0.68 eV. Comparing the latter value and the activation energy related to interface processes mechanism (0.39 eV), it can be concluded that the charge transfer process constitutes the kinetically limiting step of the whole cathode electrochemical mechanism. The relatively low value of the charge transfer activation energy suggests that there are no significant obstacles to the surface electrochemical mechanism, accordingly to the mixed ionic-electronic conductive nature of the compound proposed by Hafidi et al. [19].

4 Conclusions

A facile, easily scalable and effective synthetic route, instead of highly energetic synthetic strategies as reported in literature [15–17], is proposed as a viable preparation process for a $Na_2FeP_2O_7$/MWCNT composite and the further exhaustive electrochemical characterization has been conducted to legitimate the material mentioned above as a valid cathode material for aprotic sodium ion secondary batteries. Based on the rate tests, the surprisingly high performance of the material is highlighted. Thanks to the reliability of the compound even at high charge/discharge rates, it could also fulfill demanding application such as heavy duty secondary batteries employed in the automotive field. Behind this notable feature, the composite shows an excellent stability and high capacity retention through cycles. Apart from the mere performance aspect, with the present work we also tried to answer to the open question about the mechanism and energies involved in sodium diffusion through material–electrolyte interface and inside the material lattice. We derived values for the diffusion coefficients and activation energies from experimental evidences. To conclude, $Na_2FeP_2O_7$/MWCNT composite constitutes an extremely encouraging candidate appropriate to applications in which a high fidelity is needed. The low manufacturing costs, lastly, make this material preferable to the technologies based on Lithium, for the on grid energetic storage application.

~~Acknowledgements~~Acknowledgments

This work was supported by the Fondazione Cariplo (contract 2011-0312, “Give sodium a chance: Investigation of nanostructured mixed Na oxides as electrode materials for energy storage”) and by the Program to Solve Climate Changes (NRF-2010-C1AAA001-2010-0029031) through the National Research Foundation of Korea (NRF) funded by the Ministry of Science, ICT & Future Planning.

References

[1]

J. Hassoun, F. Bonaccorso, M. Agostini, M. Angelucci, M.G. Betti, R. Cingolani, et al., An advanced lithium-ion battery based on a graphene anode and a lithium iron phosphate cathode, *Nano Lett.* **14**, 2014, 1–17, http://dx.doi.org/10.1021/nl502429m.

[2]

M. Armand and J.-M. Tarascon, Building better batteries, *Nature* **451**, 2008, 652–657, http://dx.doi.org/10.1038/451652a.

[3]

J.B. Goodenough and Y. Kim, Challenges for rechargeable Li batteries, *Chem. Mater.* **22**, 2010, 587–603, http://dx.doi.org/10.1021/cm901452z.

[4]

J.-M. Tarascon, Is lithium the new gold?, *Nat. Chem.* **2**, 2010, 510, http://dx.doi.org/10.1038/nchem.680.

[5]

D. Larcher and J.-M. Tarascon, Towards greener and more sustainable batteries for electrical energy storage, *Nat. Chem.* **7**, 2014, 19–29, http://dx.doi.org/10.1038/nchem.2085.

[6]

L.P. Wang, L. Yu, X. Wang, M. Srinivasan and Z.J. Xu, Recent developments of electrode materials for sodium ion batteries, *J. Mater. Chem. A* 2015, http://dx.doi.org/10.1039/C4TA06467D.

[7]

Kundu et al. 2015, Angewandte Chemie International Edition, (n.d.).

[8]

R. Berthelot, D. Carlier and C. Delmas, Electrochemical investigation of the P2–Na_xCoO_2 phase diagram, *Nat. Mater.* **10**, 2011, 74–80, http://dx.doi.org/10.1038/nmat2920.

[9]

C. Didier, M. Guignard, C. Denage, O. Szajwaj, S. Ito, I. Saadoune, et al., Electrochemical Na-deintercalation from $NaVO_2$, *Electrochem. Solid State Lett.* **14**, 2011, A75, http://dx.doi.org/10.1149/1.3555102.

[10]

N. Yabuuchi, M. Kajiyama, J. Iwatate, H. Nishikawa, S. Hitomi, R. Okuyama, et al., P2-type Nax[$Fe_{1/2}Mn_{1/2}$]O_2 made from earth-abundant elements for rechargeable Na batteries, *Nat. Mater.* **11**, 2012, 512–517, http://dx.doi.org/10.1038/nmat3309.

[11]

M. Sathiya, K. Hemalatha, K. Ramesha, J.-M. Tarascon and a. S. Prakash, Synthesis, structure, and electrochemical properties of the layered sodium insertion cathode material: $NaNi_{1/3}Mn_{1/3}Co_{1/3}O_2$, *Chem. Mater.* **24**, 2012, 1846–1853, http://dx.doi.org/10.1021/cm300466b.

[12]

Y.H. Ung, C.H. Lim and D.K. Kim, Graphene-supported $Na_3V_2(PO_4)_3$ as a high rate cathode material for sodium-ion batteries, *J. Mater. Chem. A* **1**, 2013, 11350, http://dx.doi.org/10.1039/c3ta12116j.

[13]

H. Kim, I. Park, D.H. Seo, S. Lee, S.W. Kim, W.J. Kwon, et al., New iron-based mixed-polyanion cathodes for lithium and sodium rechargeable batteries: combined first principles calculations and experimental study, *J. Am. Chem. Soc.* **134**, 2012, 10369–10372, http://dx.doi.org/10.1021/ja3038646.

[14]

M. Nose, H. Nakayama, K. Nobuhara, H. Yamaguchi, S. Nakanishi and H. Iba, $Na_4Co_3(PO_4)_2P_2O_7$: a novel storage material for sodium-ion batteries, *J. Power Sources* **234**, 2013, 175–179, http://dx.doi.org/10.1016/j.jpowsour.2013.01.162.

[15]

S. Chung, Y. Yamada and A. Yamada, $Na_2FeP_2O_7$: a safe cathode for rechargeable sodium-ion batteries, *Chem. Mater.* **25**(17) 2013 3489-3487.

[16]

T. Honma, T. Togashi, N. Ito and T. Komatsu, Fabrication of $Na_2FeP_2O_7$ glass-ceramics for sodium ion battery, *J. Ceram. Soc. Jpn.* **120**, 2012, 344–346, http://dx.doi.org/10.2109/jcersj2.120.344.

[17]

T. Honma, N. Ito, T. Togashi, A. Sato and T. Komatsu, Triclinic $Na_{2-x}Fe_{1+x/2}P_2O_7$/C glass-ceramics with high current density performance for sodium ion battery, *J. Power Sources* **227**, 2013, 31–34, http://dx.doi.org/10.1016/j.jpowsour.2012.11.030.

[18]

C.-Y. Chen, K. Matsumoto, T. Nohira and R. Hagiwara, Full utilization of superior charge-discharge characteristics of $Na_{1.56}Fe_{1.22}P_2O_7$ positive electrode by using ionic liquid electrolyte, *J. Electrochem. Soc.* **162**, 2014, A176–A180, http://dx.doi.org/10.1149/2.0931501jes.

[19]

E. Hafidi, M. El Omari, M. El Omari, a. Bentayeb, J. Bennazha, a. El Maadi, et al., Conductivity studies of some diphosphates with the general formula AI2BIIP2O7 by impedance spectroscopy, *Arab. J. Chem.* 2011, 253–263,

http://dx.doi.org/10.1016/j.arabjc.2011.01.028.

[20]

H. Kim, R. a Shakoor, C. Park, S.Y. Lim, J.S. Kim, Y.N. Jo, et al., $Na_2FeP_2O_7$ as a promising iron-based pyrophosphate cathode for sodium rechargeable batteries: a combined experimental and theoretical study, *Adv. Funct. Mater.* **23**, 2013, 1147–1155, http://dx.doi.org/10.1002/adfm.201201589.

[21]

J.M. Clark, P. Barpanda, A. Yamada and M.S. Islam, Sodium-ion battery cathodes $Na_2FeP_2O_7$ and $Na_2MnP_2O_7$: diffusion behaviour for high rate performance, *J. Mater. Chem. A* **2**, 2014, 11807, http://dx.doi.org/10.1039/C4TA02383H.

[22]

Y.H. Jung, C.H. Lim, J.-H. Kim and D.K. Kim, $Na_2FeP_2O_7$ as a positive electrode material for rechargeable aqueous sodium-ion batteries, *RSC Adv.* **4**, 2014, 9799, http://dx.doi.org/10.1039/c3ra47560c.

[23]

P. Barpanda, J. Lu, T. Ye, M. Kajiyama, S.-C. Chung, N. Yabuuchi, et al., A layer-structured $Na_2CoP_2O_7$ pyrophosphate cathode for sodium-ion batteries, *RSC Adv.* **3**, 2013, 3857, http://dx.doi.org/10.1039/c3ra23026k.

[24]

C.-Y. Chen, K. Matsumoto, T. Nohira, C. Ding, T. Yamamoto and R. Hagiwara, Charge–discharge behavior of a $Na_2FeP_2O_7$ positive electrode in an ionic liquid electrolyte between 253 and 363K, *Electrochim. Acta* **133**, 2014, 583–588, http://dx.doi.org/10.1016/j.electacta.2014.04.038.

[25]

C.Y. Chen, K. Matsumoto, T. Nohira, R. Hagiwara, Y. Orikasa and Y. Uchimoto, Pyrophosphate $Na_2FeP_2O_7$ as a low-cost and high-performance positive electrode material for sodium secondary batteries utilizing an inorganic ionic liquid, *J. Power Sources* **246**, 2014, 783–787, http://dx.doi.org/10.1016/j.jpowsour.2013.08.027.

[26]

P. Barpanda, T. Ye, S. Nishimura, S.-C. Chung, Y. Yamada, M. Okubo, et al., Sodium iron pyrophosphate: a novel 3.0V iron-based cathode for sodium-ion batteries, *Electrochem. Commun.* **24**, 2012, 116–119, http://dx.doi.org/10.1016/j.elecom.2012.08.028.

[27]

E. Barsoukov and J.R. Mecdonald, Impedance Spectroscopy: Theory, Experiment and Application, 2005.

[28]

R. Ruffo, R. Fathi, D.K.J. Kim, Y.H. Jung, C.M. Mari and D.K.J. Kim, Impedance analysis of $Na_{0.44}MnO_2$ positive electrode for reversible sodium batteries in organic electrolyte, *Electrochim. Acta* **108**, 2013, 575–582, http://dx.doi.org/10.1016/j.electacta.2013.07.009.

[29]

C. Ho, Application of A-C techniques to the study of lithium diffusion in tungsten trioxide thin films, *J. Electrochem. Soc.* **127**, 1980, 343, http://dx.doi.org/10.1149/1.2129668.

[30]

K.M. Shaju, G.V. Subba Rao and B.V.R. Chowdari, EIS and GITT studies on oxide cathodes, O2-Li(2/3)+x(Co0.15Mn0.85)O2 (x = 0 and 1/3), *Electrochim. Acta* 2003, http://dx.doi.org/10.1016/S0013-4686(03)00317-7.

[31]

W. Weppner, Determination of the kinetic parameters of mixed-conducting electrodes and application to the system Li[sub 3]Sb, *J. Electrochem. Soc.* **124**, 1977, 1569, http://dx.doi.org/10.1149/1.2133112.

[32]

L. Tan, S. Zhang and C. Deng, Fast lithium intercalation chemistry of the hierarchically porous $Li_2FeP_2O_7$/C composite prepared by an iron-reduction method, *J. Power Sources* **275**, 2015, 6–13, http://dx.doi.org/10.1016/j.jpowsour.2014.10.178.

[33]

R. Tripathi, S.M. Wood, M.S. Islam and L.F. Nazar, Na-ion mobility in layered Na_2FePO_4F and olivine Na Fe,Mn PO_4, *Energy Environ. Sci.* **6**, 2013, 2257–2264, http://dx.doi.org/10.1039/c3ee40914g.

Highlights

- $Na_2FeP_2O_7$-carbon nanotubes composite is as electrode in secondary sodium batteries.
- The composite shows a stable and reversible specific capacity of 86 mA h/g at 1 C.
- The intimate contact between $Na_2FeP_2O_7$ and carbon nanotubes provides high kinetic.

Queries and Answers

Query: Please note that author's telephone/fax numbers are not published in Journal articles due to the fact that articles are available online and in print for many years, whereas telephone/fax numbers are changeable and therefore not reliable in the long term.
Answer: ok

Query: Please provide the volume number or issue number or page range for the bibliography in Refs. [15], [30].
Answer: done

Query: Please confirm that given names and surnames have been identified correctly.
Answer: given names and surnames are correct

Query: Your article is registered as a regular item and is being processed for inclusion in a regular issue of the journal. If this is NOT correct and your article belongs to a Special Issue/Collection please contact a.rassette@elsevier.com immediately prior to returning your corrections.
Answer: I confirm the paper does NOT belong to Special Issue/collection